

Photoacoustic investigation of the temperature and magnetic-field dependence of the specific-heat capacity and thermal conductivity near the Curie point of gadolinium

C. Glorieux and J. Thoen*

Laboratorium voor Akoestiek en Thermische Fysica, Departement Natuurkunde, Katholieke Universiteit Leuven, Celestijnenlaan 200D, 3001 Leuven, Belgium

G. Bednarz[†] and Mary Anne White

Department of Chemistry, Dalhousie University, Halifax, Canada B9H 4J3

D. J. W. Geldart

Department of Physics, Dalhousie University, Halifax, Canada B9H 4J3

(Received 17 April 1995)

The photoacoustic technique was used as a simple but accurate tool to simultaneously determine the specific-heat capacity C and thermal conductivity κ of gadolinium in the neighborhood of the Curie point. One polycrystalline sample and two single crystals of different quality have been investigated as a function of temperature and external magnetic field B . One of the single-crystal samples was the same as the one for which Bednarz *et al.* [Phys. Rev. B **47**, 14 247 (1993)] obtained high-resolution $C(T, B=0)$ data by means of ac calorimetry. Our photoacoustic results are in full agreement with the Bednarz *et al.* data, thus confirming the complex crossover behavior found by these authors. The photoacoustic results in the presence of low external fields clearly were affected by demagnetization effects resulting in the occurrence of kink temperatures in the $C_B(T)$ curves below the Curie temperature. Information on the temperature dependence of the spontaneous magnetization could be deduced from the experimentally obtained kink temperatures. Scaling properties for the B dependence of the specific-heat capacity have also been investigated. The thermal conductivity $\kappa(T)$ for $B=0$ shows a clear minimum at the Curie point for the best sample. The minimum is diminished with poorer sample quality and in the presence of an external magnetic field.

I. INTRODUCTION

The rare-earth metal gadolinium has many unique properties. At room temperature, gadolinium undergoes a second-order ferromagnetic-to-paramagnetic phase transition. Among the rare earths, gadolinium has the highest magnetic moment, due to the presence of several unpaired electrons in the $4f$ orbital. The isotropic S state of the magnetic spins, which are well screened from the crystal field by isotropic $5d$ and $6s$ electrons, suggests isotropic spin-spin interactions. The ferromagnetic character of gadolinium is believed to be mainly caused by these isotropic, short-range exchange interactions between nearest neighbors. Gadolinium is, however, also characterized by an anisotropic hexagonal crystal symmetry, which causes a small anisotropic term in the Hamiltonian. Anisotropy information can in principle be obtained directly from the orientation dependence of order-parameter data, or indirectly from the symmetry properties of the universality class, which can be derived from the values of the critical exponents which describe the behavior of the physical properties near the critical or Curie temperature (around room temperature). The presence of these weak anisotropic perturbations on the dominant isotropic exchange interactions is expected to influence significantly the critical behavior of gadolinium sufficiently close to the Curie point, and to result in a pattern of crossover behavior. Critical-point phenomena in gadolinium are consequently quite complex

and in spite of many experimental and theoretical studies of a variety of physical properties a detailed understanding is not yet complete.

Several authors find the experimental behavior of gadolinium to be anisotropic. Neutron-diffraction results¹ and nuclear-relaxation studies² pointed out anisotropic magnetic properties. Magnetization measurements³ showed the existence of an easy axis of magnetization. The angle between this axis and the hexagonal c axis varies from 30° at 10 K to 65° at 183 K, and becomes zero for temperatures higher than 232 K. The order-parameter anisotropy was confirmed by susceptibility measurements.⁴

In view of the strong isotropic exchange interaction, which is expected to dominate the weak anisotropic crystal influence, the significant anisotropy in the experimentally determined magnetic properties of gadolinium is rather surprising. The influence of crystal anisotropy on the spin states cannot be due to direct spin-orbit coupling, since the angular momentum of the S -state spins is zero. There are, however, other interaction contributions which are anisotropic. The important role of the Rudermann-Kittel-Kasuya-Yosida (RKKY) interaction⁵ is clearly illustrated by the experimental value of the magnetic moment, $m_{\text{expt}} = 0.794\mu_B$, which is larger than the theoretical value, $m_{\text{th}} = gS\mu_B = 7\mu_B$ (with g the gyromagnetic ratio). This excess magnetization is believed to result from a spin-polarized electron contribution. Consequently, since the conduction-electron states are

strongly influenced by the crystal-field anisotropy, they act as a significant source of anisotropy of the magnetic moments. Also dipolar interactions are believed to play an important role in the magnetic properties of gadolinium. These interactions have an isotropic part which decreases with distance as $1/r^3$ (with r the distance between two dipoles) and an anisotropic part which decreases as $1/r^5$. Since dipolar interactions have a much longer range than the very localized direct exchange interaction, they become important when the correlation length increases, thus close to the critical temperature. According to Geldart and Richard⁶ and Fujiki, De'Bell, and Geldart⁷ dipolar interactions play a crucial role in the critical behavior of gadolinium, resulting in crossover behavior.^{8,9} Recently, renormalization-group calculations¹⁰ for such systems found a complex temperature dependence of the effective critical exponent $\gamma_{\text{eff}}(t)$ (with $t=|T-T_c|/T_c$): far away from T_c , the value of γ_{eff} is Heisenberg-like, while approaching T_c the effective critical exponent changes towards uniaxial or isotropic dipolar values.

Experimental indications of crossover behavior in gadolinium were found in susceptibility measurements of Geldart *et al.*,⁴ resistivity measurements of Geldart *et al.*,¹¹ and muon-depolarization-rate experiments of Dalmas de Réotier and Yaouanc.¹² Also the critical behavior of the specific-heat capacity, which has been thoroughly investigated,¹³⁻¹⁷ could only be interpreted in the framework of complex crossover behavior between different regimes.¹⁷

Besides the theoretical complexity of the critical behavior of gadolinium, there are also several experimental aspects which render the analysis complicated. Experimental results have also illustrated that the critical behavior can vary strongly, depending on the circumstances during the annealing process.¹⁸ Experimental rounding of the data close to T_c seems to be inevitable in phase-transition investigations on solids. This rounding is mainly caused by impurities and crystal strain, rather than by temperature gradients resulting from the technique employed. More fundamental reasons for the difficult analysis of the critical behavior of gadolinium were given by Bednarz, Geldart, and White.¹⁷ Renormalization-group and other theoretical results are always deduced for single crystals. However, as a consequence of the energy gain which accompanies a multidomain configuration, real samples are always composed of several differently oriented magnetic domains. The influence of the limited size of domains is important when the correlation length becomes comparable to the dimensions of the domains and thus close enough to T_c . According to Bednarz and co-workers,^{17,18} this effect only becomes significant for $t < 10^{-4}$; thus less than 0.03 K away from T_c . Also, demagnetization effects have to be avoided as much as possible.¹⁸

The thermal properties of gadolinium have been investigated repeatedly in the past. Specific-heat capacity measurements have been carried out by ac calorimetry^{14,16,17} as well as by adiabatic calorimetry.^{13,15} Thermal-conductivity data have been obtained with static gradient methods,¹⁹⁻²¹ often by combining thermal-diffusivity results with specific-heat capacity data of different experiments and samples.^{22,23} Although the thermal behavior of Gd near the Curie point has attracted a good deal of attention, many aspects of it are not yet fully characterized and understood.

The present study involves high-resolution simultaneous measurements of the specific-heat capacity and the thermal conductivity of three gadolinium samples near the Curie point by means of the photoacoustic technique. One of the samples is polycrystalline and the others are single crystals. One of these single-crystal samples is the high-quality crystal which was also studied in detail by Bednarz, Geldart, and White¹⁷ by means of ac calorimetry. We have carried out measurements as a function of temperature for different values of an external magnetic field. In Sec. II we give a brief description of our photoacoustic setup allowing the simultaneous measurement of the specific-heat capacity C and the thermal conductivity κ . The results obtained for C and κ are discussed in Sec. III and summarized in Sec. IV.

II. EXPERIMENTAL DETAILS

Provided that the proper measuring configuration is chosen the photoacoustic technique²⁴ allows for the simultaneous determination of the specific-heat capacity and thermal conductivity. In our measuring configuration the sample, which is in contact with air on the top and bottom sides, was illuminated by a light beam with periodically modulated intensity $I=I_0\exp(i\omega t)$, with $\omega=2\pi f$ and f the modulation frequency. In such a configuration, the detected complex temperature oscillation amplitude for an optically very opaque sample (which is the case for Gd at He-Ne laser wavelength of 633 nm) is given by²⁵

$$\theta_0(\omega) = \frac{(1-R)I_0}{2\sqrt{\pi f}(1+i)e_s} \frac{\exp(\sigma_s l_s) + \exp(-\sigma_s l_s)}{\exp(\sigma_s l_s) - \exp(-\sigma_s l_s)} \quad (1)$$

with R the sample reflectivity, $e_s=(\rho_s C_s \kappa_s)^{1/2}$ the sample effusivity, l_s the sample thickness, $\sigma_s=(1+i)/\mu$, and $\mu=[a_s/(\pi f)]^{1/2}=[\kappa_s/(\pi f \rho_s C_s)]^{1/2}$ the thermal diffusion length. a_s , κ_s , ρ_s , and C_s are, respectively, the thermal diffusivity, the thermal conductivity, the density, and the specific-heat capacity of the sample. The photoacoustic pressure signal, which is produced by the piston effect of a thin, periodically heated (and thus expanding) air layer close to the sample surface, is simply proportional to the temperature oscillation and can be detected by a microphone. The magnitude and phase of the temperature oscillation can be obtained from the microphone signal via a calibration procedure in which the signal is compared to the signal of a reference sample with known optical and thermal properties (e.g., carbon-coated copper). Via an iterative calculation, Eq. (1) can be inverted in order to give the effusivity and diffusivity of the sample, from which the specific-heat capacity and thermal conductivity can easily be derived.

We have used a standard photoacoustic setup²⁵ to determine the temperature and magnetic-field dependence of the specific-heat capacity and thermal conductivity of gadolinium in the neighborhood of the Curie temperature (between 0 and 40 °C). In order to assess the influence of the sample quality on the critical behavior of the thermal properties, we have studied samples of three different qualities. Sample 1 was cut ($0.25 \times 5 \times 9$ mm³) from a 99.9% pure polycrystalline gadolinium foil obtained from Johnson and Matthey (U.K.) Sample 2 was a 365 μm thick, 8 mm diameter single-crystalline disk delivered by Metal Crystals and

Oxides (U.K.). During production, this sample was first formed by stretching a gadolinium rod, formed from doubly sublimated 99.99% pure gadolinium, which was melted by rf induction. The rod was afterwards annealed for 16 h in pure argon, 200 K below the melting point (± 1600 K) and cut by means of spark erosion. Our sample 3 is the same high-purity single-crystalline sample II studied by Bednarz, Geldart, and White¹⁷ by means of ac calorimetry. The dimensions of this sample are $0.22 \times 4.2 \times 7.4$ mm³. Further details on this sample can be found in Ref. 17. For both single-crystal samples the hexagonal *c* axis is perpendicular to the largest surface.

The photoacoustic signal was produced by illuminating the sample top surface by a 10 mW helium-neon laser beam (633 nm), which was periodically modulated by an Intraaction type AOM40 acousto-optic modulator. The signal was detected by a Brüel and Kjær type 4165 microphone followed by a type 2607 amplifier and a PAR 5210 lock-in detector and, after calibration, converted to the surface temperature making use of Eq. (1). Since the calibration procedure only allows for the determination of relative changes in the measured quantities, we have made use of reference data for gadolinium at 40 °C in order to scale the curves of the thermal properties. The specific-heat capacity $C_s(40 \text{ °C}) = 220 \text{ J kg}^{-1} \text{ K}^{-1}$ was taken from the work of Bednarz, Geldart, and White,¹⁷ while the density $\rho_s = 7890 \text{ kg m}^{-3}$ and thermal conductivity $\kappa_s = 9 \text{ W m}^{-1} \text{ K}^{-1}$ at this temperature are average values from several sources in the literature.^{19–23}

The temperature of the photoacoustic cell was automatically controlled with an accuracy better than 0.01 K, and was varied with a rate of 0.02 K/min during temperature scans. The cell temperature was measured with a thermistor calibrated against a platinum resistance thermometer which was calibrated against the international temperature scale by the National Physical Laboratory (U.K.). Within the resolution (± 0.05 K) of a sensitive mercury thermometer no change in the calibration of the thermistor was observed at periodic checks. The magnitude of the magnetic field, oriented parallel to the sample surface, was measured by a Hall probe, and controlled by automatically positioning permanent magnets around the photoacoustic cell on a foam bottom. The beam width was 4 mm, large enough to fulfill the conditions of one-dimensional heat transport, which are supposed in the theory.²⁴ Thermal effects from the optical window were avoided by choosing the length of the air column above the sample equal to 4 mm, much larger than the typical diffusion length (0.8 mm at 10 Hz modulation frequency). The “drum effect,”²⁶ which shows up when a periodically heated sample is clamped, was avoided by placing the sample on a plasticine ring.

A necessary condition for the experimental investigation of phase transitions is that measurement-induced thermal gradients are minimal. In our setup, the maximum temperature oscillation can be directly calculated from Eq. (1) and was equal to 13 mK in the worst case (800 W m⁻² light intensity at 10 Hz modulation frequency), which is smaller than the applied temperature step. The static gradient was calculated from measured T_c values at different power values, and corresponded, for 10 mW laser power, to a temperature difference of 260 mK between the measured temperature and the real sample temperature. Since this temperature dif-

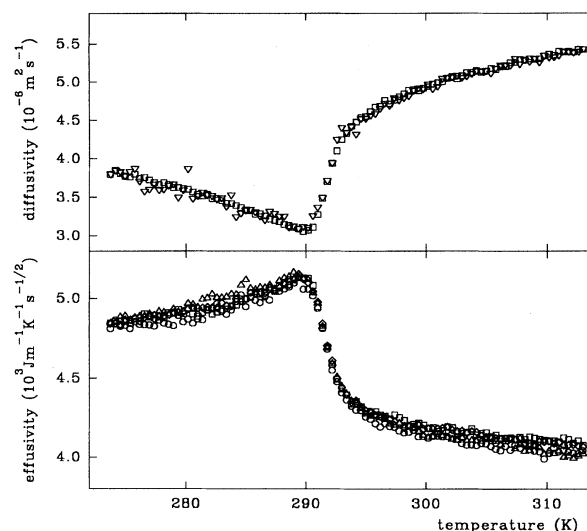


FIG. 1. Results for the thermal diffusivity and effusivity as a function of temperature for sample 2 as calculated from the photoacoustic signal amplitude and phase results for different modulation frequencies. Solid dots: 10 Hz, inverted open triangles: 15 Hz, solid squares: 60 Hz, open squares: 120 Hz, and open triangles: 240 Hz.

ference was mainly due to the thermal gradient over the poorly conducting plasticine ring ($\kappa_s/\kappa_{\text{plast}} \approx 100$), the static gradient over the sample was significantly smaller (< 20 mK) than the total temperature difference with the sample cell. The difference was nearly constant for the whole temperature range, resulting in a small temperature offset in the results.

In a separate experiment, the thermal diffusivity was measured using a non-steady-state, periodic heating method.²⁷ The heater was a layer of bismuth evaporated on one surface of the Gd sample (sample II of Bednarz, Geldart, and White,¹⁷ sample 3 here); this surface was insulated from the heater by ca. 4 μm layer of General Electric low-temperature varnish. The sample was heated at a frequency of 28 Hz, rms power 1.4 mW. The phase and amplitude of the temperature oscillations were detected on the surface opposite the heater, using a miniature thermistor.²⁸ The thermal diffusivity a was obtained from the phase reading of the lock-in amplifier, ϕ ,

$$\phi = l_s(\pi f/a_s)^{1/2} + \phi_{\text{th}} + \pi/4, \quad (2)$$

where ϕ_{th} is an unknown phase shift due to the thermal resistance of the thermometer. The unknown phase shift ϕ_{th} from this method was calculated at 275 and 315 K using the diffusivity data obtained here from the photoacoustic experiments; its value was found to be a few tens of degrees.

In an effort to check the consistency of the theoretical model, we have determined the temperature dependence of the thermal properties of sample 2 from the photoacoustic signal, using different modulation frequencies. Figure 1 shows that the curves, obtained at 10, 15, 60, 120, and 240 Hz (from a thermally thin to a thermally thick regime) are

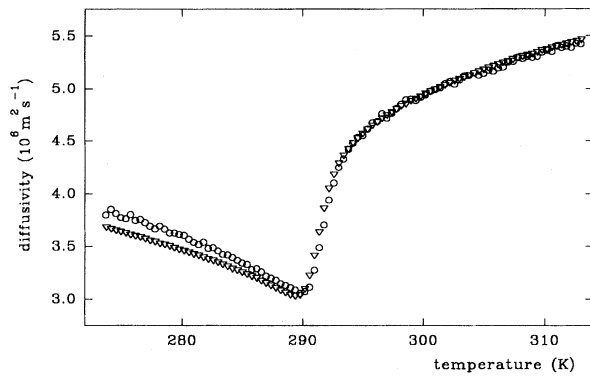


FIG. 2. Comparison of the temperature dependence of the thermal diffusivity of sample 2 as obtained by means of the photoacoustic technique (circles) and the photopyroelectric technique (triangles).

overlapping within the experimental uncertainty, confirming the validity of Eq. (1) for our configuration. This is not a surprise, given the simplicity of the contactless setup: the temperature oscillation is only determined by sample properties, and thus is independent of other materials, border conditions, etc. Perhaps even more convincing evidence for the reliability of the results is the good accordance of our data with data obtained by other techniques on the same samples. In Fig. 2 there is quite good agreement between the sample 2 diffusivity data obtained by our photoacoustic setup and by means of a photopyroelectric setup.^{25,29} The thermal diffusivities measured by the periodic heating method [Eq. (2)] confirm but underestimate the dip in the diffusivity at T_c ; the source of error is likely tied to the uncertainty in the phase shift due to thermal resistance of the thermometer. Moreover, our photoacoustic heat-capacity data for sample 3 are within the experimental uncertainties the same as the ac calorimetry data for the same sample obtained by Bednarz, Geldart, and White¹⁷ (see Fig. 3). The small systematic deviations at low

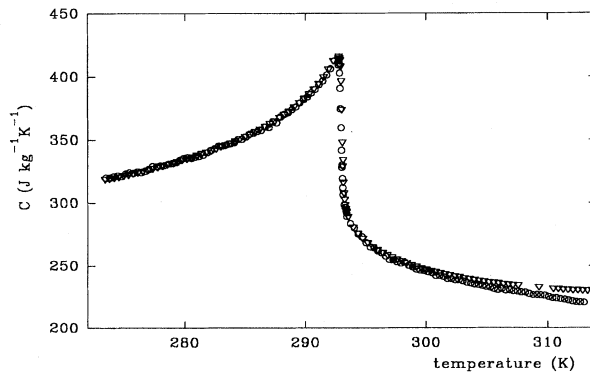


FIG. 3. Comparison of the temperature dependence of the specific-heat capacity of sample 3 determined photoacoustically (circles) and from ac calorimetry (triangles) by Bednarz, Geldart, and White (Ref. 17).

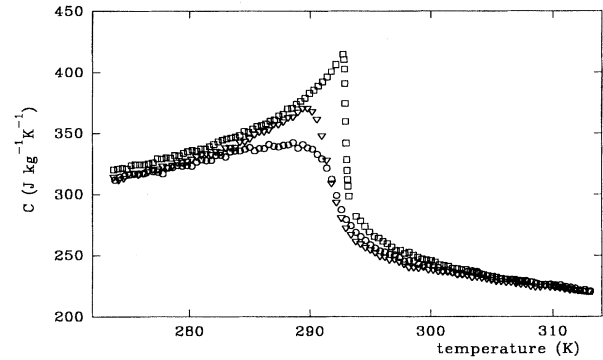


FIG. 4. Photoacoustic data for the temperature dependence of the specific-heat capacity of the samples 1 (circles), 2 (triangles), and 3 (squares), in the neighborhood of the Curie point.

temperatures in Fig. 2 and at high temperatures in Fig. 3 are the result of small errors in the slope of the calibration curves. In Fig. 2 the data points at 40 °C were superimposed and in Fig. 3 the same was done at 0 °C, because our method allows only the measurement of relative changes with temperature and magnetic field (see further). In Fig. 3 the data of Bednarz, Geldart, and White¹⁷ have been shifted downwards by $\Delta T = 1.6$ °C in order to make the C maxima in both data sets coincide.

III. RESULTS AND DISCUSSION

A. Specific-heat capacity

1. Results for zero external magnetic field

As already pointed out above, photoacoustic measurements result in data for the specific-heat capacity C and for the thermal conductivity κ . We will first discuss the C results which were obtained as a function of temperature and external magnetic field.

In Fig. 4 specific-heat capacity results are given for the three different samples in the absence of an external magnetic field. The importance of sample quality is illustrated in this figure. There is a clear correlation between the sharpness of the specific-heat-capacity anomaly and the crystalline quality of the sample. Rounding poses a severe constraint on the analysis of asymptotic behavior. As a consequence, high quality of the sample is a minimum condition for investigations of critical behavior. Sample II of Bednarz, Geldart, and White¹⁷ (our sample 3) seems to be one of the best, if not the best, in this respect and does not show evidence of rounding for $|t| > 10^{-3}$. Unfortunately, in practice, it is very difficult to separate crossover effects from rounding effects.

In view of the severe rounding observed for samples 1 and 2 in Fig. 4, an analysis in terms of a power law with the critical exponent α would only make sense for the results for the high-quality sample 3. However, such a complete analysis was already carried out by Bednarz, Geldart, and White¹⁷ for their ac calorimetry C data. Since our photoacoustically obtained C results for sample 3 are essentially a confirmation of the ac calorimetry data, a reanalysis would be redundant.

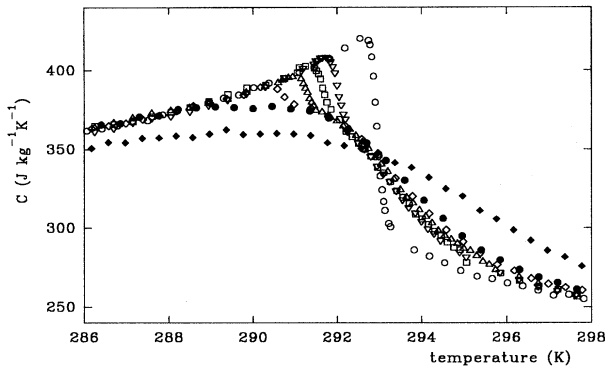


FIG. 5. Isofield curves for the specific-heat capacity of sample 3 for different values of the external magnetic field B in the neighborhood of the Curie point. Circles: 0 mT, inverted open triangles: 35 mT, open squares: 39 mT, open triangles: 43 mT, open diamonds: 48 mT, solid dots: 56 mT, and solid diamonds: 139 mT.

Bednarz, Geldart, and White¹⁷ confirmed the complexity of the experimental behavior of gadolinium, which is a consequence of both complex crossover behavior and experimental aspects (multidomain formation, stress, and demagnetization). The authors found the critical behavior of the specific-heat capacity to be Heisenberg-like, although with significant deviations from the ideal behavior, which are believed to result from crossover to dipolar behavior close to T_c .

2. Results for magnetic-field values $B \neq 0$

In the above-discussed results, the critical point ($T=T_c$, $B=0$) was approached along a line of constant magnetic field $B=0$. In order to get a better insight into the critical behavior, it can be interesting to approach the critical point via another route in the parameter space, e.g., by applying a changing magnetic field at constant temperature $T=T_c$. Simons and Salamon¹⁵ already performed a detailed investigation of the influence of a magnetic field by measuring the isofield curves $C_B(T)$ for different values of B . Their results represent a good base of comparison for our data.

In Fig. 5 the temperature dependence of the specific-heat capacity of sample 3 is shown for different values of a magnetic field which was applied parallel to the sample surface and thus perpendicular to the hexagonal c axis. As the magnetic field increases, the specific-heat capacity anomaly becomes less pronounced, because of the increasing distance to the critical point. For temperatures higher than T_c , the influence of the magnetic field on the specific-heat capacity decreases with increasing temperature. This is in agreement with the decreasing magnetic susceptibility $\chi(T, B)$, which reflects the decreasing influence of the magnetic field on the order parameter (i.e., the magnetization) and consequently on the specific-heat capacity. Below T_c , with decreasing temperature, the influence of the magnetic field on the specific-heat capacity changes rather abruptly at a so called "kink" temperature T_k . This effect is due to the presence of a demagnetizing field, as was pointed out by Griffiths.³⁰ The demagnetizing field is caused by magnetic moments at the

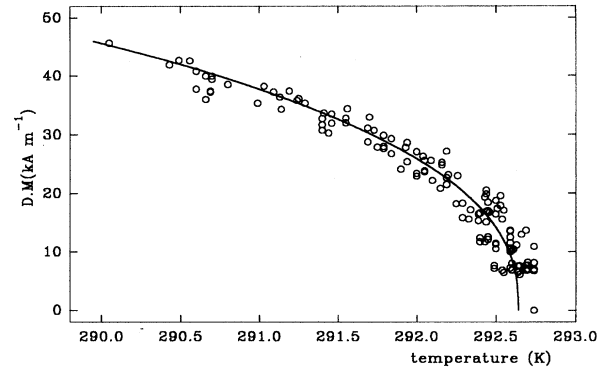


FIG. 6. Temperature dependence of DM_s (with M_s the spontaneous magnetization and D the demagnetization factor) below T_c , determined from the kink temperatures in $C_B(T)$ curves. The solid curve result from a power-law fit to the data (see text).

sample surface, which are not internally compensated, and depends on the form factor D , which is determined by the shape of the sample. Because of this demagnetization effect, the effective internal magnetic field B_{in} is smaller than the externally applied field B :

$$\begin{aligned} B_{in} &= B - \mu_0 DM & \text{for } B > \mu_0 DM \\ &= 0 & \text{for } B \leq \mu_0 DM, \end{aligned} \quad (3)$$

with M the magnetization and $\mu_0 = 1.26 \times 10^{-6}$ H/m the permeability of vacuum. Since the magnetization increases with decreasing temperature, the external field becomes more and more screened. Therefore the influence of the external field on the spins, and hence on the specific-heat capacity, decreases. From the kink temperature on, the magnetization gets so large that the internal influence of the external field is completely neutralized by the demagnetizing field. Unfortunately, this demagnetization effect makes it impossible to study the influence of a magnetic field on the specific-heat capacity if the temperature or the magnetic field is too low. However, it offers an unexpected tool to determine the spontaneous magnetization M_s in an indirect way. Since the kink temperature represents the starting temperature for complete demagnetization, it is characterized by the condition $B = \mu_0 DM$. Thus for different kink temperatures one can write

$$M_s(T_k) = B(T_k) / \mu_0 D. \quad (4)$$

Since μ_0 and D are constant, the $B(T_k)$ curve is proportional to the spontaneous magnetization $M_s(T_k)$. In Fig. 6 results for $DM_s(T_k) = B(T_k) / \mu_0$ as derived for T_k values from the kinks in the $C_B(T)$ curves for different external magnetic field choices are given. According to phase-transition theory, the temperature dependence of M_s should follow a power-law behavior of the form

$$M_s(T, B=0) = M_0 |t|^\beta, \quad (5)$$

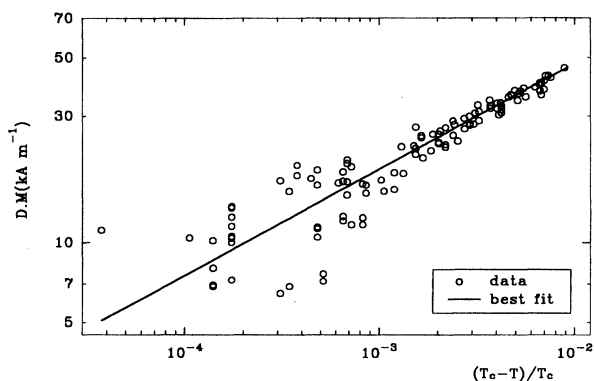


FIG. 7. Double-logarithmic plot of the DM_s data of Fig. 6. The straight-line results form a power-law fit with a critical exponent $\beta = 0.40 \pm 0.17$.

with M_0 and β , respectively, the critical amplitude and critical exponent. From a least-squares analysis of the DM data of Fig. 6 we found $T_c = 292.6 \pm 0.2$ K, $\beta = 0.40 \pm 0.17$, and $DM_0 = (3.0 \pm 2.7) \times 10^5$ A m $^{-1}$. This β value is the same value as given by Chowdhury, Collins, and Hohenemser,³¹ which was obtained from $\gamma\gamma$ angular correlation experiments. In Fig. 7 the experimental data and the best fit are compared in a double-logarithmic plot. The rather large standard deviations on the adjustable parameters are mainly caused by the uncertainty in deriving the kink temperature from the always somewhat rounded $C_B(T)$ curves (see Fig. 5). Although a reasonable value is obtained for the critical exponent β , the uncertainty is too large to attribute a specific universality class.

For large enough external magnetic fields we can neglect the influence of the demagnetization effect and try to describe simultaneously the B and T dependence of $C_B(T)$ results on the basis of scaling properties of the equation of state. A rescaling approach has been applied by many authors^{32–38} in the past for several magnetic phase transitions, including the Curie point of gadolinium. In particular, parametric equations of state, satisfying the scaling-law relations, predict the following scaling behavior:^{37,38,15}

$$\hat{C}(B, T) h^{-\alpha/\beta\delta} = g(th^{1/\beta\delta}), \quad (6)$$

with $\hat{C}(B, T) = C(B, T) - C(B=0, T)$, $h = (7.94\mu_B/k_B T_c)B$ (μ_B is the Bohr magneton and k_B the Boltzmann constant), g a universal curve, and δ the critical exponent characterizing the $M(B)$ behavior of the critical isotherm at the critical point. In Fig. 8 our scaled specific-heat-capacity data $C_B(T)$ for sample 3 obtained for different B values, which were chosen large enough to minimize demagnetization effects, are compared. The curves coincide quite well when the scaling is performed according to Ising exponent values for the critical exponents.³⁹ However, scaling shows some improvement with theoretical Heisenberg exponent values.³⁹ Since our experimental data are in good agreement with similar data for gadolinium obtained by Simons and Salamon,¹⁵ we also scaled our data using values for the ex-

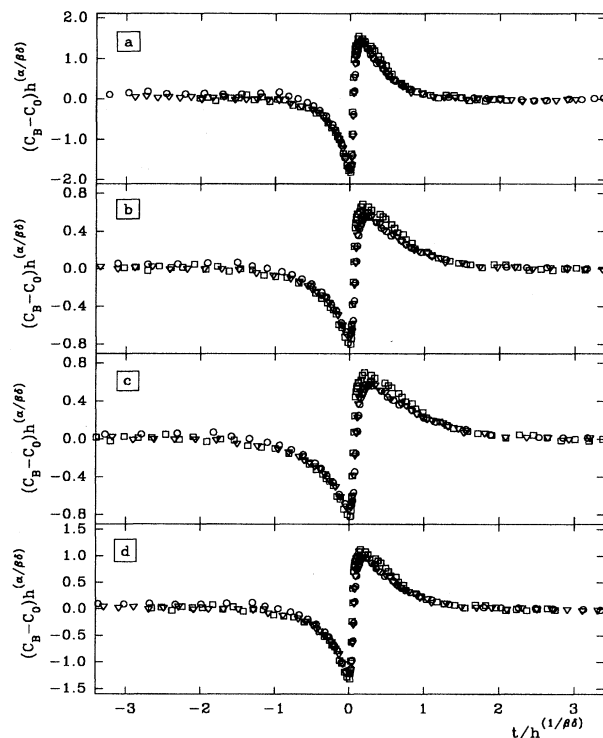


FIG. 8. Scaled [according to Eq. (6)] $C_B(T)$ curves for sample 3 using theoretical critical exponents for the Heisenberg model (a), the Ising model (b), and effective critical exponents ($\alpha=0.1$, $\beta=0.4$, and $\delta=3.75$) of Simons and Salamon (Ref. 15) (c), or a set of literature values selected by us ($\alpha=-0.02$, $\beta=0.39$, and $\delta=4.18$) (d). Curves for different external magnetic-field values are given by open circles for $B=60$ mT, triangles for $B=75$ mT, and squares for $B=139$ mT.

ponents which were proposed by these authors. The rather special choice of critical exponents ($\alpha=0.1$, $\beta=0.4$, $\delta=3.75$) was made in order to obtain the best fit of their data to the “linear model” of Schofield³³ and Ho.³⁴ Simons and Salamon¹⁵ also noticed a large difference between the amplitude of the scaled data and that of the theoretical curve. This can be due to either the limited quality of the sample, or the complex crossover behavior of gadolinium. Probably also the linear model is too simple to account for all aspects of the magnetic equation of state.

In an effort to optimize the scaling data collapse on a single curve, we also have scaled our data using the following experimentally determined (effective) critical exponent values from the literature:^{17,40–43} $\alpha=-0.02$, $\beta=0.39$, and $\gamma=1.20$. A value for δ was derived from the relation $\delta=(2-\alpha)/\beta-1=4.18$. This scaling also leads to coinciding $C_B(T)$ curves, of a similar quality as in the case of scaling with theoretical Heisenberg exponents. The most important common feature between the two sets of exponents is the negative (Heisenberg-like) sign of α . The slightly better quality in these two cases is, however, not convincing enough to draw straightforward conclusions concerning the universality class of gadolinium. The good overlap after scal-

ing in all four cases is an interesting confirmation of the concept of the scaling of the magnetic equation of state.

B. Thermal conductivity

In the early years of phase-transition investigations, theoretical research was focused on static physical properties like specific-heat capacity, magnetization, density, etc. More recently, the increased availability of experimental data for the critical behavior of dynamic properties has stimulated the theoretical efforts in the field of critical dynamics. This has, for example, led to the mode-coupling theory.⁴¹ Most of the transport properties are directly or indirectly influenced by material order, and thus also by order-parameter fluctuations, resulting in critical behavior.

Concerning heat transport, two dynamic properties are important, the thermal conductivity and the thermal diffusivity, and they are simply related via heat capacity and density. One could ask which of the two quantities is more relevant for the study of critical dynamics. The thermal diffusivity automatically shows up when the thermal-diffusion equations are solved for time-variant heat input. Although in such cases the thermal conductivity can only be found indirectly (combining thermal diffusivity with effusivity or heat capacity), κ is coupled more directly to microscopic material properties. Moreover, κ appears automatically when one derives the heat-transport equation as the (phenomenological) proportionality constant between heat flux and temperature gradient. Most theories which describe heat transport starting from microscopic properties lead to the thermal conductivity. According to the Debye theory for heat transport, the isotropic phonon thermal conductivity is determined by the phonon specific heat capacity C_{ph} , the mean free path l_{ph} of the phonons, and the mean phonon velocity v_{ph} :

$$\kappa_{ph} = \frac{C_{ph} v_{ph} l_{ph}}{3}. \quad (7)$$

In metals κ is coupled also to the electrical conductivity $\sigma_e = 1/\rho_e$ (ρ_e is the electrical resistivity) via the Wiedemann-Franz law.⁴⁴ One should also remark that by considering the diffusivity $a = \kappa/\rho C$ the specific-heat capacity does not disappear from the Debye equation for κ , since both κ and C consist of several components for each energy-carrying "particle" (e.g., phonons, electrons, magnons). Consequently, expressions for a are not simpler than the ones for κ . In Sec. II we already pointed out that from the photoacoustic measurements one can derive accurate and reliable results for κ from diffusivity and effusivity ($\kappa = e\sqrt{a}$). We will thus consider here the thermal conductivity in order to discuss the critical behavior of heat transport.

For gadolinium $\kappa(T)$ data in literature are rather limited. Moreover, there are considerable differences between different data sets. Also, no clear picture of a possible critical behavior seems to emerge from existing data. The resolution in the results of Meis, Froment, and Moulinier²³ was too limited to derive information on the critical behavior. Chuah and Ratnalingam²⁰ and Nellis and Legvold¹⁹ found a minimum at 270 K in the a -axis thermal conductivity, while the c -axis conductivity did not show any anomaly at T_c . Other authors found a slight change of slope for $\kappa(T)$ at T_c . The most extensive study of the thermal conductivity of gado-

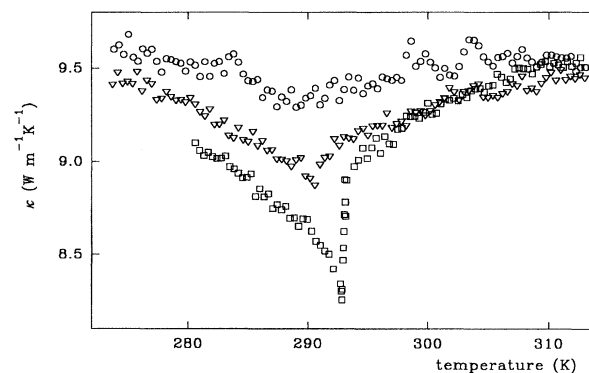


FIG. 9. Photoacoustic data for the temperature dependence of the thermal conductivity of samples 1 (circles), 2 (triangles), and 3 (squares) in the neighborhood of the Curie temperature.

linium was performed by Jacobsson and Sundqvist.²² They found a minimum in $\kappa(T)$ at the critical temperature. Since, in order to determine the thermal conductivity, the authors had to combine diffusivity and specific-heat-capacity results of different samples and in view of the large temperature difference over the samples during the measurements (5 K), the resolution of their results is limited. Several reasons can be given to explain this diversity in the experimental results. Stationary methods often suffer from systematic deviations and a low resolution. Moreover, most of the results were obtained for polycrystalline samples, resulting in severe rounding of a possible critical anomaly and in an average over κ_c and κ_a , the c - and a -axis thermal-conductivity values. In many cases results were obtained from a combination of diffusivity and heat-capacity data for different samples, which reduces the reliability substantially near T_c , especially since the thermal conductivity is the product of the thermal diffusivity (which shows a dip at T_c) and the heat capacity (which shows a peak at T_c).

The importance of sample quality for the investigation of the critical behavior of the thermal conductivity of gadolinium is clearly illustrated in Fig. 9. With increasing crystal quality the anomaly, a minimum in $\kappa(T)$ at T_c , becomes more and more pronounced. Although the critical effect in $\kappa(T)$ is limited (less than 15%), we believe that, in view of the high resolution of these photoacoustic data and the different reliability tests we earlier described, there is no reason to doubt the presence of the minimum.

Since there exist different heat-transport mechanisms in magnetic metals, it is difficult to make quantitative theoretical predictions of $\kappa(T)$. In most materials, the main part of heat transport is carried by phonons, and is limited by phonon-phonon collisions. Usually, the Debye approximation for phonon heat transport leads to accurate predictions of the temperature dependence of κ_{ph} . Typical for the metal gadolinium is also the considerable contribution of conduction electrons to the heat transport.^{5,22} This heat-conduction mechanism is related to electric conduction, in a simple relation between the electron thermal conductivity κ_e and the electrical conductivity σ_e (the Wiedemann-Franz law⁴⁴). In

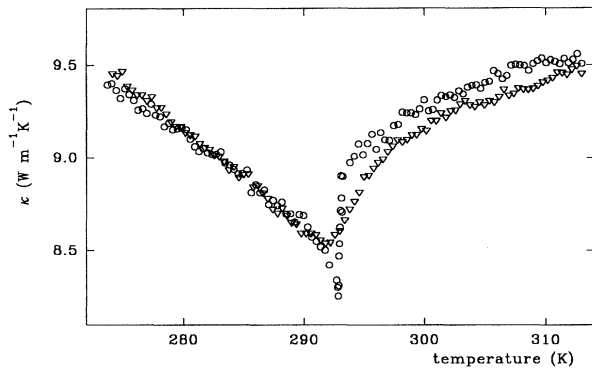


FIG. 10. Effect of a magnetic field on the thermal conductivity of sample 3 in the neighborhood of the Curie temperature. Circles are for $B=0$ and triangles for an external field $B=60$ mT.

most metals the heat transport is dominated by conduction electrons, resulting in a similar behavior of $\kappa(T)$ and $\sigma_e(T)$. In magnetic materials a third heat-transport mechanism is possible via magnons.⁵ The transport of magnetic energy is carried by a spin-wave quantum or magnon, made possible by combined spin-spin interactions, which can act to restore a thermodynamic equilibrium situation and thus as a heat-wave mechanism. This effect is similar to the direct and inverse magnetocaloric effect, in which magnetic-field changes cause temperature changes and conversely temperature changes induce magnetization changes.

The thermal conductivity of the ferromagnetic metal gadolinium thus can be written as $\kappa = \kappa_{\text{ph}} + \kappa_e + \kappa_{\text{mag}}$. In principle, all three contributions may be responsible for a minimum at T_c . The limiting factor for phonon heat conduction is the phonon-phonon collisions. The possibility exists that the strongly increasing spin disorder at T_c has, via spin-orbit coupling, an influence on the electron orbital moment and indirectly on the lattice and its vibration modes. The existence of significant interactions between the spins and the lattice by which the spin temperature is kept equal to the lattice temperature via spin-spin interactions is shown by nuclear magnetic and electron spin resonance experiments. In gadolinium, however, the spin-orbit coupling is zero because of the zero orbital moment but the spin-lattice energy exchange can also happen via the exchange interaction and via conduction electrons. The thermal transport in gadolinium is to a large extent carried by conduction electrons. Also this kind of heat conduction can in principle exhibit critical behavior. Consequences of the RKKY interaction or indirect exchange interaction (playing an important role in rare earths) are an effective mass enhancement of conduction electrons by localized spins and a change of the density of states at the Fermi surface.⁵ In this way spin disorder can have an indirect influence on κ_e . Because of the Wiedemann-Franz law κ_e is expected to be inversely proportional to the electrical resistivity and one can learn about the thermal conductivity from the electrical resistivity behavior. Although more limited, the c -axis resistivity peak seems to be in qualitative agreement with the minimum in our data for the c -axis thermal conductivity. The existence of a peak in

the c -axis resistivity is rather surprising, since the Fisher-Langer⁴⁵ theory predicts only a slope change at T_c . Different explanations were given for this discrepancy. According to Zumsteg *et al.*⁴⁶ the disagreement between Fisher-Langer predictions and the experimental data is due to a lattice contraction at T_c . Geldart *et al.*¹¹ tried to model the resistivity behavior by a crossover from Heisenberg to uniaxial dipolar behavior.

Although the thermal conductivity of gadolinium is dominated by the conduction electrons, and to a lesser extent by phonons, the $\kappa(T)$ minimum at T_c could best be explained due to the increasing spin-wave scattering when T_c is approached. Unfortunately, it is difficult to experimentally determine the magnon contribution to the thermal conductivity. However, an effort to explain the global $\kappa(T)$ behavior, combining the three contributions, led to a reasonable result.²²

Assuming an increasing scattering of energy-carrying particles for $T \rightarrow T_c$, the reduction of the $\kappa(T)$ anomaly (Fig. 10) because of the presence of a magnetic field becomes plausible. With increasing magnetic field, the distance to the critical point increases, causing a decreasing influence of fluctuations on the energy carriers. The absence of influence below a certain temperature can again be explained by demagnetization effects, similarly to the specific-heat-capacity data.

IV. SUMMARY AND CONCLUSIONS

In this paper we described the results of a photoacoustic investigation near the ferromagnetic-to-paramagnetic phase transition of the rare-earth metal gadolinium. We have shown that the photoacoustic technique allows the simultaneous measurement of the specific-heat capacity C and the thermal conductivity κ . Both the temperature and magnetic-field dependence of C and κ have been investigated for three samples of different quality.

From a comparison of the results for the three samples, we confirmed previous observations that rounding effects can only sufficiently be avoided for very high-quality single-crystal samples, like our sample 3, which was previously also investigated by Bednarz, Geldart, and White¹⁷ by means of high-resolution ac calorimetry. The photoacoustically obtained specific-heat data for sample 3 in zero magnetic field are in full agreement with the ac calorimetry results of Bednarz, Geldart, and White,¹⁷ thus confirming the high-resolution capabilities of the photoacoustic technique. Since our data confirm those of Bednarz, Geldart, and White¹⁷ they render further support to the conclusions of these authors on the complex crossover behavior of the specific-heat capacity as a function of temperature on approaching the Curie point.

We have also carried out a detailed study of the specific-heat capacity $C_B(T)$ for many values of the external magnetic field B . The isofield $C_B(T)$ curves at low magnetic-field values clearly showed a so-called "kink" temperature T_k below the Curie temperature caused by demagnetization effects. The kink temperature can be ascribed to demagnetization effects related to the shape of the sample. From the T_k values for many $C_B(T)$ curves indirect information could also be obtained on the temperature dependence of the spontaneous magnetization and thus on the critical exponent β for

which a value of 0.40 ± 0.17 was obtained from a fit with a simple power-law equation.

Using a parametric equation of state approach, the $C_B(T)$ data for larger fields (where the impact of demagnetizing effects is reduced) could be well scaled to a single curve. However, it turned out that more than one set of critical exponents gave a good scaling result.

For the c -axis thermal conductivity of the high-quality sample 3 in zero magnetic field a clear minimum was observed at the Curie temperature. It was also found that, for poorer sample quality or by applying an external magnetic field, the minimum is substantially reduced or even disappears. For the thermal conductivity in gadolinium three different transport mechanisms are considered to be relevant: phonon, conduction-electron, and magnon heat transport. Ar-

guments can be put forward in each case to allow for a dip in the thermal conductivity at the Curie point. At this point it is, however, not clear which plays the dominant role, if indeed they are separable.

ACKNOWLEDGMENTS

This work was supported by the Belgian National Science Fund (NFWO) through an FKFO project (No. 2.0043.91), by the European Commission in the framework of a Human Capital and Mobility Network Program (Contract No. ERBCHRXCT930365), by the Natural Science and Engineering Research Council of Canada (M.A.W. and D.J.W.G.), and by the Killam Foundation (G.B.).

* Author to whom correspondence should be addressed.

† Present address: Long Hospital, L-75, Box 0226, University of California, San Francisco, CA 94143.

¹H. R. Child, *Phys. Rev. B* **18**, 1247 (1978).

²G. S. Collins, A. R. Chowdhury, and C. Hohenemser, *Phys. Rev. B* **33**, 4747 (1986).

³F. Milstein and L. B. Robinson, *Phys. Rev.* **177**, 177 (1969).

⁴D. J. W. Geldart, P. Hargraves, N. M. Fujiki, and R. A. Dunlap, *Phys. Rev. Lett.* **62**, 2728 (1989).

⁵J. Jensen and A. R. Mackintosh, *Rare Earth Magnetism* (Clarendon, Oxford, 1991).

⁶D. J. W. Geldart and T. G. Richard, *Phys. Rev. B* **12**, 5175 (1975).

⁷N. M. Fujiki, K. De'Bell, and D. J. W. Geldart, *Phys. Rev. B* **36**, 8512 (1987).

⁸M. E. Fisher and A. Aharony, *Phys. Rev. Lett.* **30**, 559 (1973).

⁹A. Aharony and M. E. Fisher, *Phys. Rev. B* **8**, 3323 (1973).

¹⁰K. Ried, Y. Millev, M. Fähnle, and H. Kronmüller, *Phys. Rev. B* **49**, 4315 (1994).

¹¹D. J. W. Geldart, K. De'Bell, J. Cook, and M. J. Laubitz, *Phys. Rev. B* **35**, 8876 (1987).

¹²P. Dalmas de Réotier and A. Yaouanc, *Phys. Rev. Lett.* **72**, 290 (1994).

¹³M. Griffel, S. Skochdopole, and F. H. Spedding, *Phys. Rev.* **93**, 657 (1954).

¹⁴E. A. S. Lewis, *Phys. Rev. B* **1**, 4368 (1970).

¹⁵D. S. Simons and M. B. Salamon, *Phys. Rev. B* **10**, 4680 (1974).

¹⁶P. C. Lanchester, J. A. Potton, and D. P. Baker, *Phase Transitions* **6**, 59 (1985).

¹⁷G. Bednarz, D. J. W. Geldart, and M. A. White, *Phys. Rev. B* **47**, 14 247 (1993).

¹⁸G. Bednarz and D. J. W. Geldart, *J. Phys. Condens. Matter* **5**, L239 (1993).

¹⁹W. J. Nellis and S. Legvold, *Phys. Rev.* **180**, 581 (1969).

²⁰D. G. S. Chuah and R. Ratnalingam, *J. Low Temp. Phys.* **14**, 257 (1974).

²¹J. B. Sousa, R. P. Pinto, M. M. Amado, M. F. Pinheiro, J. M. Moreira, and M. E. Braga, *J. Phys. (Paris)* **41**, 573 (1980).

²²P. Jacobsson and B. Sundqvist, *Phys. Rev. B* **40**, 9541 (1989).

²³C. Meis, A. K. Froment, and D. Moulinier, *J. Phys. D* **26**, 560 (1993).

²⁴A. Rosencwaig and A. Gersho, *J. Appl. Phys.* **47**, 64 (1976).

²⁵C. Glorieux, Ph.D. thesis, Katholieke Universiteit Leuven, 1994.

²⁶P. Charpentier, F. Lepoutre, and L. Bertrand, *J. Appl. Phys.* **53**, 608 (1982).

²⁷G. C. Danielson and P. H. Sidles, in *Thermal Conductivity*, edited by R. P. Type (Academic, New York, 1969), Vol. 2.

²⁸G. Bednarz, B. Millier, and M. A. White, *Rev. Sci. Instrum.* **63**, 9541 (1992).

²⁹A. Mandelis and M. M. Sver, *J. Appl. Phys.* **57**, 4421 (1985).

³⁰R. B. Griffiths, *Phys. Rev. B* **188**, 942 (1969).

³¹A. Chowdhury, G. S. Collins, and C. Hohenemser, *Phys. Rev. B* **33**, 6231 (1986).

³²M. Vicentini-Missoni, J. M. H. Levelt Sengers, and M. S. Green, *Phys. Rev. Lett.* **22**, 389 (1969).

³³P. Schofield, *Phys. Rev. Lett.* **22**, 606 (1969).

³⁴J. T. Ho, *Phys. Rev. Lett.* **26**, 1485 (1971).

³⁵C. C. Huang and J. T. Ho, *Phys. Rev. A* **7**, 1304 (1973).

³⁶R. Krasnow and H. E. Stanley, *Phys. Rev. B* **8**, 332 (1973).

³⁷M. Barmatz, P. C. Hohenberg, and A. Kornblit, *Phys. Rev. B* **12**, 1947 (1975).

³⁸P. Schofield, J. D. Litster, and J. T. Ho, *Phys. Rev. Lett.* **23**, 1098 (1969).

³⁹J. C. Le Guillou and J. Zinn-Justin, *J. Phys. (Paris) Lett.* **46**, 137 (1985).

⁴⁰J. W. Cable and E. O. Wollan, *Phys. Rev. B* **165**, 733 (1968).

⁴¹P. C. Hohenberg and B. I. Halperin, *Rev. Mod. Phys.* **49**, 435 (1977).

⁴²M. N. Deschizeaux and G. Develey, *J. Phys. (Paris)* **32**, 319 (1971).

⁴³G. H. J. Wentenaar, S. J. Campbell, D. H. Chaplin, T. J. McKenna, and G. V. H. Wilson, *Phys. Rev. B* **29**, 1419 (1984).

⁴⁴C. Kittel, *Introduction to Solid State Physics* (Wiley, New York, 1976).

⁴⁵M. E. Fisher and J. S. Langer, *Phys. Rev. Lett.* **20**, 665 (1968).

⁴⁶F. C. Zumsteg, F. J. Cadieu, S. Marcelja, and R. D. Parks, *Phys. Rev. Lett.* **25**, 1204 (1970).